Nuclear Materials and Energy 12 (2017) 989–993

Contents lists available at ScienceDirect

Nuclear Materials and Energy

journal homepage: www.elsevier.com/locate/nme

Fast imaging of filaments in the X-point region of Alcator C-Mod

J.L. Terry[a,*], S. Ballinger[b], D. Brunner[a], B. LaBombard[a], A.E. White[a], S.J. Zweben[c]

[a] MIT Plasma Science and Fusion Center, 175 Albany St., Cambridge, MA 02139, USA
[b] Columbia University, New York, NY 10027, USA
[c] Princeton Plasma Physics Laboratory, Princeton, NJ 08543, USA

ARTICLE INFO

Article history:
Received 14 July 2016
Revised 12 October 2016
Accepted 20 November 2016
Available online 27 January 2017

Keywords:
Alcator C-Mod
Turbulence
Divertor
X-point
Filaments

ABSTRACT

A rich variety of field-aligned fluctuations has been revealed using fast imaging of D_α emission from Alcator C-Mod's lower X-point region. Field-aligned filamentary fluctuations are observed along the inner divertor leg, within the Private-Flux-Zone (PFZ), in the Scrape-Off Layer (SOL) outside the outer divertor leg, and, under some conditions, at or above the X-point. The locations and dynamics of the filaments in these regions are strikingly complex in C-Mod. Changes in the filaments' generation appear to be ordered by plasma density and magnetic configuration. Filaments are not observed for plasmas with $n/n_{Greenwald} \lesssim 0.12$ nor are they observed in Upper Single Null configurations. In a Lower Single Null with $0.12 \lesssim n/n_{Greenwald} \lesssim 0.45$ and Bx∇B directed down, filaments typically move up the inner divertor leg toward the X-point. Reversing the field direction results in the appearance of filaments outside of the outer divertor leg. With the divertor targets "detached", filaments inside the LCFS are seen. These studies were motivated by observations of filaments in the X-point and PFZ regions in MAST, and comparisons with those observations are made.

1. Introduction

Filaments, also known as blobs, have been observed in the boundaries of tokamak plasma for many years. Considerable attention has been paid to their generation and dynamics (see [1] and references therein). They have been shown to be strong fluctuations of density, temperature, and potential localized perpendicular to the magnetic field and approximately aligned with the magnetic field, i.e. "field-aligned". They are called "filaments" because of this structure, which causes them to appear as extended filaments when viewed in a way that exposes their 3D geometry. They appear as localized "blobs" when viewed roughly parallel to the magnetic field. The characteristic time-scales for the lifetimes of these fluctuations are 10–100 μs. Most of the work with filaments involves observations on the low-field, bad-curvature side of toroidal plasmas, since they are readily generated and typically observed there. Filaments extending from the low-field-side boundary of the main plasma into the divertor have also been imaged and studied on NSTX [2,3], MAST [4], and C-Mod [5]. More recently there have been observations in MAST of filaments along the divertor legs and in the PFZ [6,7]. These MAST observations, the relative scarcity of experimental study and simulation work in this area, and the fact that very little about these *divertor-leg* filaments is understood has motivated the research described here. In addition to the desire to understand these phenomena, there is the motivation that the filaments may provide a mechanism for moving heat and particles away from the strike points, for fueling the main plasma, or for increasing transport generally in this region, thereby explaining increased transport often needed in modeling the inner divertor distributions of temperature and density [8]. Thus, additional detailed study, including fast imaging, is warranted.

Sections 2 and 3 describe the experimental arrangement and the techniques used to locate the filaments in space and follow them in time. Section 4 relates details of the filament dynamics in C-Mod under various conditions. Section 5 compares the C-Mod results with the observations from MAST, discusses implications of the observations for fueling the core/main plasma, and briefly hypothesizes about possible explanations for the filament dynamics. Section 6 presents a short summary of the principal findings.

2. Experimental arrangement and registration of the camera's view

The optical system that images emission from the lower X-point region is mounted on the outer wall of the Alcator C-Mod

* Corresponding author.
E-mail address: terry@psfc.mit.edu (J.L. Terry).

http://dx.doi.org/10.1016/j.nme.2016.11.020

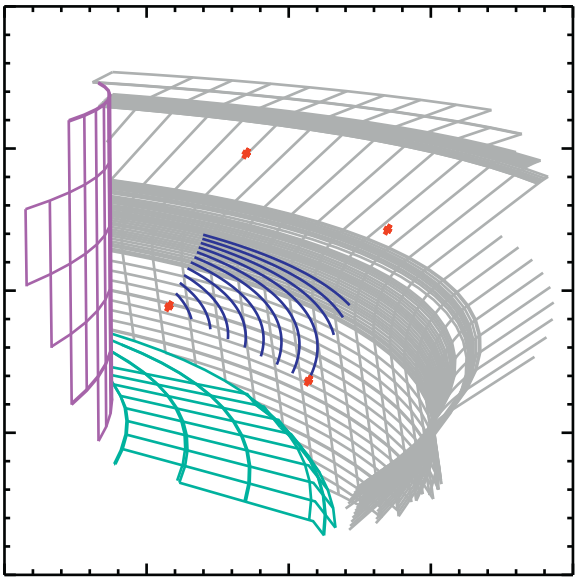

Fig. 1. System's view of the lower X-point region in C-Mod is marked by the 4 red crosses. The outer divertor target is shown with the grey lines, the inner target shown with the purple lines, and the floor of the inner target is shown with light blue-green lines. Shown in dark blue are toroidally symmetric line segments in a single horizontal plane that pierce the system's view. (For interpretation of the references to color in this figure legend, the reader is referred to the web version of this article.)

vacuum vessel. It consists of a polished stainless steel mirror that directs the light upward through two achromats and 19 mm diameter vacuum window onto a coherent bundle of quartz fibers. The 5 m long fiber bundle is in atmosphere within a long flexible bellows (O.D. 19 mm) that is re-entrant from a vacuum flange at the top of C-Mod and has been routed in-vessel to place the input face of the fiber bundle at the focus of the in-vacuum optical system. The other end of the coherent bundle is routed to a Phantom V710 fast-framing camera mounted atop C-Mod. Coupling of the plasma light output from 4 mm × 4 mm coherent bundle onto the camera's detector-array is accomplished by de-magnifying the bundle area by a factor of 3 using two camera objective lenses, between which is a D_α bandpass interference filter. The 64×64 pixel sub-window of the camera's detector-array is read out at 390,804 frames per sec with integration times selected between 1 and 2.1 μs, depending upon emission intensity.

The object focal plane of the in-vessel optical system is roughly where the view is tangential to the field-lines piercing that plane. The view is also angled down by 11° with respect to horizontal. The system's view of the plasma-facing armor tiles on the inner and outer divertor targets and on the central column has been reconstructed using the registration technique described below and is shown in Fig. 1. Emission from anywhere along the camera's lines-of-sight are imaged with differing resolution depending upon the system's depth-of-field; thus it is hard to assign single value for the spatial resolution. In the object focal plane of the in-vessel optics the resolution is ∼ 1 mm, while in the far and near fields of the optics we estimate that the resolution is better than 5 mm.

Because we have a 3D view projected upon the 2D image plane of the optical system, we have carefully registered the view in order to determine how 3D features, e.g. field-aligned filaments, appear in the images. The registration procedure, which was carried out during manned-access inside the vessel, entailed placing, in-vessel, 0.56 m lengths of 6 mm diameter light sources that were formed into toroidal symmetric lines at measured (R, Z) locations, where (R, Z) are the major radius and height relative to the midplane, i.e. vessel/plasma coordinates. These light sources were then imaged by the system, and the images were compared with the computer-generated model of the view and the "line" light sources in their known locations as in Fig. 1, where 11 such modeled "line" sources are shown in blue. The view was adjusted in the model until there was an excellent match between the measured registration images and the images predicted by the model.

3. Image analysis

There is considerable D_α-emission from the divertor regions. Most of it is only slowly varying compared the typical turbulent-fluctuation timescales and compared to the fast frame rates used here. Therefore, in order to increase the contrast of the fluctuating emission, we employed two types of "background" subtraction. In some cases we found the *minimum* signal for each pixel during the nearest (in time) N frames and subtracted those values from the frame being considered. N was typically 8–20. In other cases we subtracted the *average* for each pixel for the nearest M frames, where M was typically 5–20. An example of a plasma image for which the minimum-subtraction was used is shown in Fig. 2a.

Precise knowledge of the view in plasma coordinates (see Section 2) allows reconstruction of images of what field-aligned emission structures, i.e. field-aligned filaments, would look like. We assume that the features we see in the experiment are aligned with the local magnetic field and of roughly constant emission parallel to the field. We then construct a set of "basis" images from an array of simulated field-aligned D_α-emitting filaments. This "basis" set consists of a grid of possible field-aligned filaments that on first pass would appear within the system's field-of-view. The geometry of the possible filaments comes from the EFIT [9] reconstruction for the discharge and time of interest, and such a grid of possible filaments is shown in Fig. 3 by the regular array of small open circles. The "basis" images for the two filaments piercing the (R,Z) coordinates marked with the green circles in Fig. 3 are shown in Fig. 2b and c and are matched to an actual (background-subtracted) plasma image (Fig. 2a) exhibiting filaments at those locations. Each of the basis images is unique, so that identification of a measured filament-feature with a basis image locates that filament in the R,Z plane.

4. Filament dynamics

Since the set of basis images allows us to locate the observed filaments in the R,Z plane, we can then follow the dynamics of the filaments by tracking them over sequential frames. To date this matching and tracking has been done mostly "by hand", meaning that the basis image that best matches the feature in a plasma image is chosen by eye, and then that feature is followed frame by frame for its lifetime. This labor-intensive quantitative procedure, illustrated in Figs. 2 and 3, has been carried out for a limited number of plasma image sequences. Those sequences that we have analyzed "by hand" are characteristic of filament motions that were found to be similar after viewing a large number of image sequences from a large number of discharges. We find that different types of characteristic filament generation and dynamics organize by magnetic topology and roughly by plasma density, normalized density ($n/n_{Greenwald}$), or collisionality. (We have not at this time determined which of these different density measures best organizes the differences.) We find that filament generation and motion depend on divertor magnetic configuration (USN, LSN, limited) and whether the $B \times \nabla B$ drift direction is toward or away from the active X-point. We also find filament generation increases with plasma density/normalized density/collisionality. Below we present these results in categories distinguished by the magnetic configuration. We observe filament generation and propagation

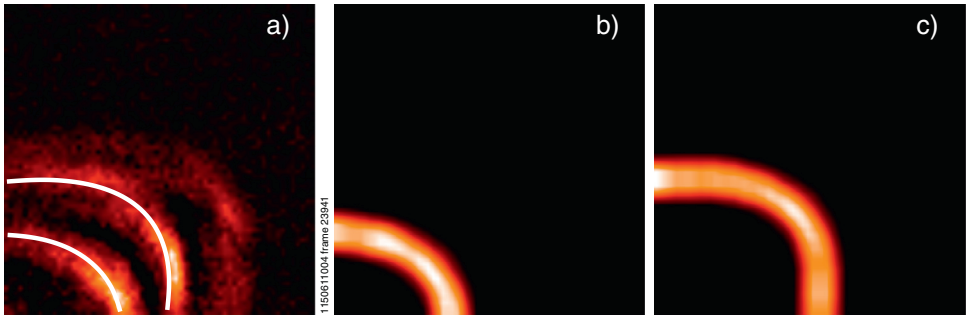

Fig. 2. a) An actual plasma image (background-subtracted) with filaments matching the shapes of the two "basis" images in b) and c). The superimposed thin white lines are the centers of two basis images. A third filament is also apparent in the plasma image. b) The reconstructed image for a field-aligned filament piercing the R,Z plane at the location of the lower-left green-circle in Fig. 3. c) The reconstructed image for a field-aligned filament piercing the R,Z plane at the location of the upper-right green circle in Fig. 3. (For interpretation of the references to color in this figure legend, the reader is referred to the web version of this article.)

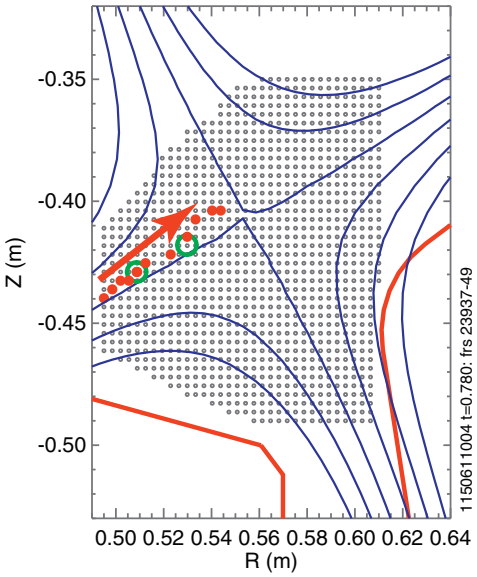

Fig. 3. Cross-section of C-Mod's lower divertor region. The array of small open circles shows the R,Z locations of the "basis" set of filaments. The two green circles are the locations for 2 filaments found in a single plasma frame and shown in Fig. 2a. The outer "vertical" target is the red line on the right. The inner divertor floor of is the red line on the left. Flux-surface contours from the EFIT reconstruction at the time of the measurements are shown in blue. The red dots and red arrow indicate the trajectory of a filament tracked in sequential plasma frames and showing upward motion along the inner leg, as discussed in Section 4.2. (For interpretation of the references to color in this figure legend, the reader is referred to the web version of this article.)

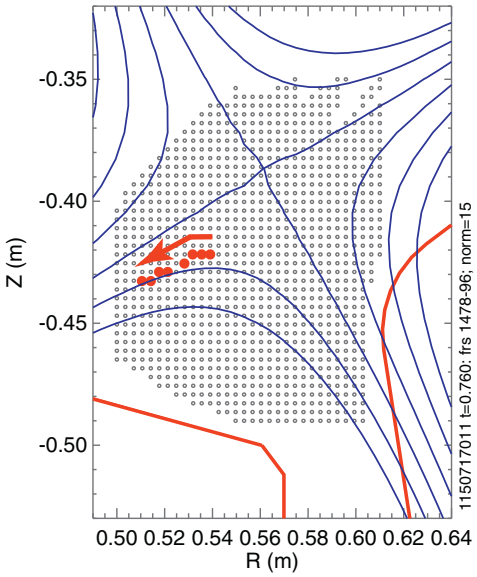

Fig. 4. Cross-section of C-Mod's lower divertor region. The red dots are the locations for a filament found in 18 sequential plasma frames showing its inward and downward motion within the PFZ. The open circles show the R,Z locations of the "basis" set of filaments. (For interpretation of the references to color in this figure legend, the reader is referred to the web version of this article.)

in this region in all confinement modes, L-mode, H-mode (EDA, ELM-free, and ELMy), and I-mode.

4.1. Upper Single Null magnetic topology

In USN configurations we typically observe no filaments. This is also true when the plasma is limited on the inner wall, and implies that the presence of a lower primary X-point may be necessary for filament generation in the lower divertor region. In these USN cases we also do not see evidence of filaments, which are observed to exist in the midplane region on the low-field bad-curvature side, wrapping around the bottom of the plasma.

4.2. Lower Single Null magnetic topology with the Bx∇B drift direction towards the X-point

We have examined a number of different cases in LSN. The most typical in C-Mod is with the Bx∇B drift direction towards the lower X-point and $n/n_{Greenwald}$ in the range 0.1–0.45. For $n/n_{Greenwald} \gtrsim 0.17$, we typically see filaments generated low along the inner divertor leg and propagating up the inner leg towards the X-point. These filaments appear to be at the inner leg or within the SOL near the inner leg. We assert that the motion is poloidal and not the result of toroidal rotation of filaments tilted with respect to horizontal, and postpone the reasons for this assertion until Section 4.3. The typical motion up along the inner leg SOL is illustrated in Fig. 3, where the red dots are the sequential locations for filament features tracked in sequential plasma images for a plasma with $n/n_{Greenwald} \sim 0.2$. (There are other filaments in the same image sequence that we have not tracked.) Assigning the filament location to a region within the magnetic configuration (for example, within the inner SOL as in Fig. 3 or in the PFZ as in Fig. 4) requires the knowledge of the equilibrium, as reconstructed here using EFIT. We estimate the accuracy of the EFIT-reconstructed strike-point locations to be +/−6 mm on the inner target and +/−10 mm on the outer target, based upon measurements of the location of the peak in the target heat-flux (from IR thermography), as well as measurements of the location of the peak in the electron pressure at the target (from arrays of embedded probes). In the instance illustrated in Fig. 3 the filament persisted for ∼30 μs as it entered the view and then moved up the inner leg toward the X-point at 1.9 km/s. Typical speeds are 1–2 km/s.

Under these conditions filaments are generated along the inner legs at rates of roughly 20,000/s. (This rate can be highly variable for reasons still unknown. It is evaluated by counting excursions of background-subtracted 400-frame time histories from single pixels that are greater than 0.6 times one standard deviation from the mean of the time history. Other than this evaluation, there is no other *quantitative* criterion for what constitutes a filament.) In the lower density plasmas, the lifetimes of the filaments tend to be smaller, the filaments tend to be less distinct, and they do not propagate as far up the inner leg. For plasmas with $n/n_{Greenwald} \lesssim 0.17$ the filaments appear to stagnate, i.e. exhibit very little motion during their lifetimes. In plasmas with values of $n/n_{Greenwald} \lesssim 0.12$ (which is $\overline{n_e} \sim 8 \times 10^{19}$ m^{-3} for C-Mod at $I_p = 0.8$ MA), we observe *no filaments* either on the inner leg or in the SOL outboard of the outer leg. Even though the D_α emission is significantly smaller in the low density LSN cases as well as in the USN cases, we do not attribute the absence of filaments under these conditions to signal-to-noise limitations in the emission. However, if the relative fluctuation measure, $\frac{\tilde{I}}{I}$, is significantly reduced with density, then we are less able to assert the absence of filaments (although this also raises the issue of what constitutes a filament).

Under the more typical conditions of moderate density, we also observe, though much less frequently than the inner-leg filaments, filaments *in the PFZ* moving radially inward and downward. This is shown in Fig. 4. The speed for this type of filament dynamic is slower, $V_R^{fil} \sim -0.6$ km/s. The downward motion is qualitatively similar to the divertor filament motion seen in MAST. We have not made a quantitative evaluation of the occurrence frequency of these PFZ filaments.

4.3. Lower Single Null magnetic topology with the Bx∇B drift direction away from the X-point

By reversing the toroidal field direction, Bx∇B is directed away from the lower X-point. Filaments tracking up near the inner leg are still seen some in "reversed-B" conditions. However filaments moving upward in the SOL of the outer leg are now apparent. Many things change under these "reversed-B" conditions, including more heat directed to the inner target and less to the outer target [10], so it is still not clear what the primary cause is for the appearance of filaments in the outer-leg SOL. These observations are illustrated in Fig. 5, where the same sequence of frames yields filaments following the two trajectories shown. The inner-leg filament speeds and trajectories do not differ significantly from those in "normal-B" conditions, i.e. speeds are in the 1–2 km/s range; however the outer-leg filaments are slower, with $V_Z^{fil} \lesssim 0.6$ km/s. In plasmas for which Bx∇B is up *and the inner target is hot*, i.e. $T_e^{target} > 20$ eV, we see *only* outer-leg filaments, i.e. no inner-leg filaments, in which case, the filament trajectories and speeds are similar to the one shown on the right in Fig. 5.

As noted in Section 4.2, we routinely observe filaments moving up the inner leg (Fig. 3) at the same time that filaments in the PFZ are moving down and radially inward (Fig. 4). The field-lines associated with R,Z coordinates of these trajectories are tilted in the *same* direction with respect to horizontal. The two trajectories shown in Fig. 5 (both upward and occurring at the same time) are associated with field-lines that tilt in *opposite* directions. A rigid toroidal rotation cannot produce these effects, hence our assertion that the motion we deduce is primarily poloidal.

4.4. Lower Single Null magnetic topology with both targets detached

In cases when the targets are fully detached, i.e. pressure is no longer constant along B and the temperatures at the target are <5 eV, and a MARFE has moved to the X-point, filaments appear both in the outer SOL and in *closed-flux-surface regions* above the X-point. The filament lifetimes are shorter than those under conditions reviewed in Sections 4.2 and 4.3. The filaments also display different directions of motion. These observations are illustrated in Fig. 6, for which the tracked filament in the SOL (green trajectory) moves down, while the filament inside the LCFS moves up and in (red trajectory). These tracks are just two of many filaments observed for this discharge under these conditions.

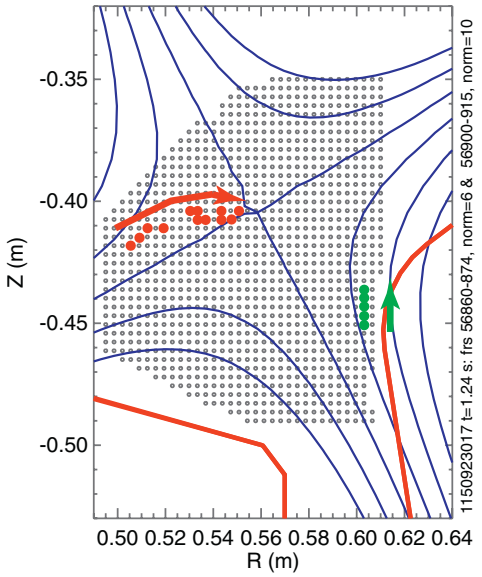

Fig. 5. Cross-section of C-Mod's lower divertor region showing filament trajectories typical of plasmas with Bx∇B away from the X-point. The red dots are the locations for a filament found in 14 sequential plasma frames showing its upward motion along the inner leg, while the green dots show the trajectory in the same sequence of a filament in the SOL of the outer divertor leg. (For interpretation of the references to color in this figure legend, the reader is referred to the web version of this article.)

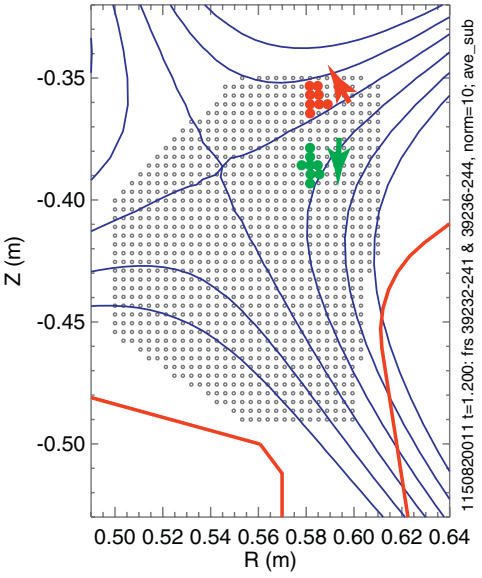

Fig. 6. The red dots are the locations for a filament found within the LCFS in 9 sequential plasma frames showing its upward and inward motion. The green dots are the locations for a filament existing at the same time in the outer SOL and moving downward. This behavior is seen in plasmas for which the divertor legs are detached and there is an X-point MARFE. (For interpretation of the references to color in this figure legend, the reader is referred to the web version of this article.)

Table 1
The MAST entries are deduced from [6,7]. ρ_i is the ion gyro-radius, assuming 10 eV for C-Mod; ν_i is the ion collision frequency. The frame rate for the C-Mod observations is 391,000 frames/s; for MAST it is 120,000 frames/s.

	C-Mod	MAST
Filament location (LSN attached conditions)	–Along inner leg –In outer leg SOL (when Bx∇B is up) –Sometimes in PFZ	–Along inner leg –Along outer leg –Into PFZ from inner leg
Filament location (LSN detached conditions with X-pt MARFE)	–Around X-point and inside LCFS	
Apparent poloidal motion at inner leg	–Upward along leg in SOL ($n/n_{Greenwald}$ >0.12) –Downward for filaments in PFZ	Downward along leg
Filament size ⊥ to B	~0.5 cm (~60 ρ_s)	~1–2 cm (~15 ρ_s)
|| Correlation length	<one toroidal transit (<3.7 m)	>one toroidal transit (>3.9 m)
Filament life-time	~10 μs (~50/ν_i)	~100 μs (~50/ν_i)

5. Discussion and comparisons with MAST observations of filaments in the X-point region

Because of the relative scarcity of observations of divertor-leg filaments and because there is much about them that is not understood, we begin the discussion of our results with a comparison to those found on the MAST spherical tokamak [6,7]. There are certainly qualitative similarities, the most obvious being that the filaments are found localized to the inner leg. But there are also differences that may lead to a better understanding. We note that collision frequencies are roughly 10x larger in C-Mod's closed divertor configuration, compared to those in MAST's open divertor. The comparison of some chosen parameters is presented in Table 1.

The dynamics of the filaments are noteworthy in their variation. The polarization-plus-bad curvature-drive responsible for the motion of filaments found in the low-field-side midplane region [11,12] does not appear to dominate the drive of these divertor-leg and PFZ filaments. Myra et al. [13] predict that *spinning* filaments drive poloidal motion that could overwhelm the polarization-drive. This mechanism could be at work here, but we have no direct evidence for this. Thus, we cannot provide a definitive explanation for the observed filament dynamics.

Because the inner-leg filaments move up toward and to the X-point, we now consider the possible effect of these filaments on main-plasma fueling. The filaments are believed to be large enhancements to the averaged local density. Thus in principle, the inner-leg filament motion could transport those particles to the X-point and into the main plasma. Furthermore, in C-Mod there is a shortfall in accounting for the main plasma fueling and the parallel flows [14], i.e. the level of neutral recycling and ionization at the inner divertor leg does not appear to be returning material back into the main plasma at a sufficient rate to match the rate at which parallel flows that bring particles from the low-field-side transport-driven source to the inner leg. Inner-leg filaments moving to the X-point provide a mechanism for convecting particles to the confined plasma. Thus we have estimated the maximum fueling rate that might be provided by the observed inner-leg filaments. The fueling shortfall in C-Mod is 10^{21}–10^{22} ions/s. We estimate the *maximum* filament fueling rate by assuming that all particles in the inner-leg filaments reach the X-point and that each filament carries the ion/electron density of measured at the inner strike-point, $\sim 2\times 10^{20}$ m^{-3}. Calculating the maximum filament fueling rate as (filament "birthrate" x filament volume x filament density), we find a rate of $\sim 5\times 10^{20}$ s^{-1}, which appears to be too low for this mechanism to be the dominant player in closing the shortfall.

Finally, we discuss possible connections between these divertor filaments and those routinely observed in the low-field-side midplane-region SOL. Because we observe no filaments in the lower divertor region in strongly-USN configurations (Section 4.1), we concluded that the low-field-side midplane filaments do not wrap around the bottom of the plasma. This implies that the filaments seen in the inner SOL during LSN operation are *not* connected with filaments in the low-field-side midplane region. The situation is less clear for the divertor filaments observed in the low-field-side SOL (Sections 4.3 and 4.4). Previous work has shown that at least some low-field-side midplane filaments in C-Mod plasmas do map magnetically through the outer SOL to probes in the outer target [5]. However, for the present observations we have no direct evidence connecting the divertor filaments with those in the midplane region.

6. Summary

Motivated by observations of filamentary fluctuations in the divertor region of MAST, we used fast-imaging of D_α light from the C-Mod divertor to examine the generation and motion of filaments there. Like MAST, we observe filaments. We see them under most conditions for which there is a lower primary X-point. Their generation rate can be tens of thousands per second. Some of the main characteristics of the C-Mod filaments are summarized in Table 1, where they are also compared with those found in MAST. We have tracked selected filaments as they move along various characteristic trajectories. The filament generation and motion depend upon the magnetic configuration (LSN, USN, or limited), the Bx∇B direction, and appear to organize roughly around the plasma density or collisionality. These observations illustrate that there is much that we still do not understand about the fluctuations and turbulence in these regions.

Acknowledgments

The authors thank James Harrison of MAST for useful conversations and his help in this research. The work was supported by DoE Contract DE-FC02-99ER54512 on Alcator C-Mod, a DoE Office of Science user facility.

References

[1] D.A. D'Ippolito, J.R. Myra, S.J. Zweben, Phys. Plasmas 18 (2011) 48 060501.
[2] R.J. Maqueda, D.P. Stotler, N. Team, Nucl. Fusion 50 (2010) 075002.
[3] F. Scotti, Private communication.
[4] N.B. Ayed, et al., Plasma Phys. Controlled Fusion 51 (2009) 035016.
[5] O. Grulke, J.L. Terry, I. Cziegler, B. LaBombard, O.E. Garcia, Nucl. Fusion 54 (2014) 043012.
[6] J.R. Harrison, G.M. Fishpool, B.D. Dudson, J. Nucl. Mater. 463 (2015) 757.
[7] J.R. Harrison, G.M. Fishpool, A.J. Thornton, N.R. Walkden, M. Team, Phys. Plasmas 22 (2015) 092508.
[8] F. Reimold, et al., J. Nucl. Mater. 463 (2015) 128.
[9] L.L. Lao, et al., Nucl. Fusion 25 (1985) 1611.
[10] R.A. Pitts, et al., J. Nucl. Mater. 337–339 (2005) 146.
[11] S.I. Krasheninnikov, Phys. Lett. A 283 (2001) 368.
[12] S.I. Krasheninnikov, D.A. D'Ippolito, J.R. Myra, J. Plasma Phys. 74 (2008) 679.
[13] J.R. Myra, D.A. D'Ippolito, S.I. Krasheninnikov, and G.Q. Yu, Phys. Plasmas 11 (2004) 4267.
[14] N. Smick, B. LaBombard, I.H. Hutchinson, Nucl. Fusion 53 (2013) 023001.